Shapes of random walks at order $1/d^2$

1991 J. Phys. A: Math. Gen. 24 2131

(http://iopscience.iop.org/0305-4470/24/9/022)

J. Phys. A: Math. Gen. **24** (1991) 2131–2149. Printed in the UK

Shapes of random walks at order $1/d^2$

Arezki Beldjenna†, Joseph Rudnick† and George Gaspari‡

† Department of Physics, University of California at Los Angeles, Los Angeles, CA 90024, USA

‡ Department of Physics, University of California at Santa Cruz, Santa Cruz, CA 95064, USA

Received 10 September 1990

Abstract. In this article we calculate various parameters which characterize the size and shape of random walks utilizing a recently developed $1/d$ expansion technique, where d is the spatial dimension in which the random walk takes place. A new procedure for extracting the averages of the principal radii of gyration is presented and the calculation is carried out to order $1/d^2$, which is one order higher than previous work. Comparison with the results of numerical simulations provides new insights regarding the accuracy of the $1/d$ expansion procedure.

1. Introduction

This paper is the continuation of our previous work on the study of shapes of random walks (see Rudnick and Gaspari (1986) and Gaspari *et al* (1987) and references therein; for an alternate approach, see Eichinger (1985) and Shy and Eichinger (1989)). As before, we limit our consideration to random walks which are not self-avoiding. The core of an analysis is the study of the resolvent, $R(\lambda)$,

$$R(\lambda) = \mathrm{Tr}\left(\frac{1}{\lambda \mathbf{I} - \mathbf{T}}\right) \tag{1}$$

of the complex variable, λ, and where $\mathbf{I}$ is the identity operator and $\mathbf{T}$ is the radius of gyration tensor (Solc 1971). Previously we were able to obtain the first two terms in a $1/d$ expansion for the average of the components of the radii of gyration, $\langle R_i^2 \rangle$. Comparison between a theoretical prediction and computer simulations done by Bishop and Michel (1985, 1986) and Bishop and Saltiel (1986) are remarkably good, the error being of the order of 5% in three dimensions. This encourages us to investigate the next higher-order term, in the hope of substantially reducing the remaining discrepancy.

Using the techniques of contour integrals, we can extract analytical expressions for the principal radii of gyration and their probability distribution function. We find that, for linear chains, the average principal radii of gyration are given by

$$\langle \lambda_i \rangle \equiv \langle R_i^2 \rangle = \frac{(N+1)}{\pi^2 i^2}\left[1 + \frac{3}{4d} + \frac{1}{d^2}\left(\frac{\pi^2 i^2}{48} - \frac{1}{32}\right)\right] + \mathrm{O}\left(\frac{1}{d^3}\right). \tag{2}$$

The ratios between the eigenvalues are, to order $1/d^2$,

$$\frac{\langle \lambda_i \rangle}{\langle \lambda_j \rangle} \equiv \frac{\langle R_i^2 \rangle}{\langle R_j^2 \rangle} = \frac{j^2}{i^2}\left(1 + \frac{1}{d^2}\frac{\pi^2}{48}(i^2 - j^2)\right). \tag{3}$$

One property of this new result is the dependence on spatial dimension of the ratios

0305-4470/91/092131+19$03.50

of the eigenvalues, which is not a property of the $O(1/d)$ results. Our new results are discussed in detail in section 4 where they are also compared with numerical simulations The agreement between the analytical expression and the results of numerical simulations for the largest principal radius of gyration is remarkably good, even at very low dimensions, such as $d=2$, $d=3$. Comparing $1/d$ expansion results with our simulations in two and three dimensions, and with the numerical results reported by Bishop and Saltiel (1986) in two to five dimensions, we find that the probable error for the largest eigenvalue is less than 2% in all dimensions.

While the $1/d$ expansion works surprisingly well at low order there is reason to believe that it is probably not mathematically well behaved. A key assumption in our analysis is almost certainly not justified in the dimensionalities of interest. This assumption is described above equation (9) and further discussed in section 4.3. The behaviour of the coefficient of $1/d^2$ in equation (3), in which either i or j may be as large as d, may be taken as an indication of potential shortcomings of the method, and is, in fact, an indication that the $1/d$ expansion is not a convergent series but an asymptotic one.

The plan of this paper is as follows. In the next section we present the basic formalism and the terminology to be used. Section 3 sketches the derivation of the $1/d^2$ correction for the analytical expression of the resolvent function $\langle R(\lambda)\rangle$. The details are presented in the appendix. The formalism which we have developed for the analysis of the resolvent function is used to calculate the principal radii of gyration. Explicit expressions for $\langle\lambda_i\rangle$ and $\langle\lambda_i^2\rangle$ are derived and presented in this section. The final section is devoted to the discussion of the $1/d^2$ results and their comparison with numerical simulations.

2. General considerations

A fundamental quantity which serves to characterize the shape of an N-step random walk is the radius of gyration tensor $\mathbf{T}$ (Solc 1971). The elements of $\mathbf{T}$ are given by

$$T_{ij}=\frac{1}{(N+1)}\sum_{l=1}^{N+1}(x_{li}-\langle x_i\rangle)(x_{lj}-\langle x_j\rangle) \tag{4}$$

where x_{li} is the ith component of the position vector of the lth vertex in the walk, and $\langle x_i\rangle$ is the average over the walk

$$\langle x_i\rangle=\frac{1}{(N+1)}\sum_{l=1}^{N+1}x_{li}. \tag{5}$$

Using the displacement vectors $\boldsymbol{\eta}_\alpha$ which connect the αth and $(\alpha+1)$th vertices, it can be shown that the elements of $\mathbf{T}$ become (Kramers 1946, Fixman 1962, Forsman and Hughes 1963)

$$T_{ij}=\sum_{\alpha,\beta=1}^{N}a_{\alpha\beta}\eta_{\alpha i}\eta_{\beta j} \tag{6}$$

where $a_{\alpha\beta}$ is a real, symmetric matrix with elements

$$\begin{aligned} a_{\alpha\beta}&=\frac{1}{(N+1)^2}\alpha(N+1-\beta) && \alpha<\beta \\ &=\frac{1}{(N+1)^2}\beta(N+1-\alpha) && \alpha>\beta \end{aligned} \tag{7}$$

and $\eta_{\alpha i}$ is the ith component of the displacement vector $\boldsymbol{\eta}_\alpha$ for the αth step.

For essentially all unrestricted walks, the probability distribution function $P(\eta_{\alpha i})$ for the chain segments $\eta_{\alpha i}$ can be taken to be Gaussian in the limit of large $N \gg 1$ (Kuhn 1936, 1939, Flory 1971). Such a walk is equivalent to a random flight with the following probability distribution for η:

$$P(\eta_{\alpha i}) = \left(\frac{d}{2\pi}\right)^{1/2} \exp\left(-\frac{d}{2}\eta_{\alpha i}^2\right)$$

d being the dimensionality. The normalization is chosen so that the average length of a link is unity, i.e.

$$\sum_{i=1}^{d} \langle \eta_{\alpha i}^2 \rangle = 1. \tag{8}$$

The fundamental quantity which will be used in our study of the shapes of random walks is the resolvent, $R(\lambda)$. Using equation (1), the fact that the imaginary part of $\langle R(\lambda) \rangle$ is the ensemble average of the probability distribution of eigenvalues of $\mathbf{T}$, some standard results of contour integration, and assuming that the resolvent and its averages are sufficiently well behaved that averages and integration operations can be commuted, we have

$$\langle \lambda_n \rangle = \frac{1}{2\pi i} \oint_{C_n} \langle R(\lambda) \rangle \lambda \, d\lambda \tag{9}$$

where C_n is a small contour which encloses λ_n. This result requires $\langle R(\lambda) \rangle$ to be analytic except for poles at the eigenvalues, which is indeed the case in high dimensions. Similarly, we have

$$\langle \langle \lambda_n^2 \rangle \rangle = \frac{1}{2\pi i} \oint_{C_n} \langle R(\lambda) \rangle \lambda^2 \, d\lambda. \tag{10}$$

Known results to first order in $1/d$ can be rederived easily using the above expressions.

2.1. Evaluation of the resolvent function $\langle R(\lambda) \rangle$

Expanding the resolvent function $R(\lambda)$ in powers of $\mathbf{T}$ we obtain

$$R(\lambda) = (\mathrm{Tr}) \frac{1}{\lambda \mathbf{I} - \mathbf{T}} = \mathrm{Tr} \frac{1}{\lambda} \left[1 + \left(\frac{\mathbf{T}}{\lambda}\right) + \frac{\mathbf{T}^2}{\lambda^2} + \dots \right] = \frac{1}{\lambda} \sum_{n=1}^{\infty} \mathrm{Tr} \left(\frac{\mathbf{T}}{\lambda}\right)^n + \frac{d}{\lambda}. \tag{11}$$

Thus,

$$\langle R(\lambda) \rangle = \frac{1}{\lambda} \sum_{n=1}^{\infty} \left\langle \mathrm{Tr} \left(\frac{\mathbf{T}}{\lambda}\right)^n \right\rangle + \frac{d}{\lambda}. \tag{12}$$

A diagrammatic method can now be used to evaluate $\langle R(\lambda) \rangle$ (Gaspari *et al* 1987). We can write

$$\mathrm{Tr}(\mathbf{T}^n) = \sum_{\substack{\alpha_1\beta_1 \\ \vdots \\ \alpha_n\beta_n}} \sum_{i_1 \dots i_n} \langle \eta_{\alpha_1 i_1} a_{\alpha_1\beta_1} \eta_{\beta_1 i_2} \eta_{\alpha_2 i_2} a_{\alpha_2\beta_2} \eta_{\beta_2 i_3} \cdots \eta_{\alpha_n i_n} a_{\alpha_n\beta_n} \eta_{\beta_n i_1} \rangle. \tag{13}$$

where the matrices $a_{\alpha_k\beta_k}$ are the same for every N-step random walk and their spectrum is very well known, with eigenvalues

$$\alpha_i = \frac{(N+1)}{\pi^2 i^2} \qquad i = 1, 2, \dots, N.$$

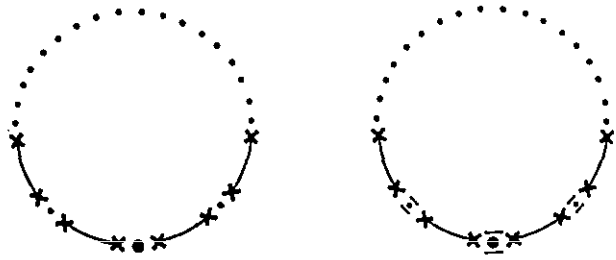

(a) (b)

Figure 1. (*a*) The representation of $\mathrm{Tr}(\mathbf{T}/\lambda)^n$. (*b*) The representation of the lowest-order contribution to $\langle \mathrm{Tr}(\mathbf{T}/\lambda)^n \rangle$.

The averages in equation (13) are thus over the ηs. Recall that the displacements corresponding to different links are statistically independent. Therefore, for linear chains,

$$\langle \eta_{\alpha i} \eta_{\beta j} \rangle = \frac{1}{d} \delta_{\alpha\beta} \delta_{ij}. \tag{14}$$

Since the distribution of the ηs is Gaussian we also have

$$\begin{aligned} &\langle \eta_{\alpha_1 i_1} \eta_{\alpha_2 i_2} \eta_{\alpha_3 i_3} \eta_{\alpha_4 i_4} \rangle \\ &\quad = \langle \eta_{\alpha_1 i_1} \eta_{\alpha_2 i_2} \rangle \langle \eta_{\alpha_3 i_3} \eta_{\alpha_4 i_4} \rangle + \langle \eta_{\alpha_1 i_1} \eta_{\alpha_3 i_3} \rangle \langle \eta_{\alpha_2 i_2} \eta_{\alpha_4 i_4} \rangle \\ &\quad\quad + \langle \eta_{\alpha_1 i_1} \eta_{\alpha_4 i_4} \rangle \langle \eta_{\alpha_2 i_2} \eta_{\alpha_3 i_3} \rangle \end{aligned} \tag{15}$$

and, in general, the average of a product of $2m$ ηs will equal a sum of products of the average of m pairs of ηs. The sum is over the $(2m)!/2^m m!$ distinct ways of constructing m pairs of the $2m$ ηs.

A diagrammatic method has been introduced to keep track of the pairings of ηs. This method can be used to systematize the $1/d$ expansion. The details of the graphical method are given in a previous paper, and we refer the reader to that work (Gaspari *et al* 1987) for specifics. Here we directly apply the technique to the calculation of $\langle R(\lambda) \rangle$.

As an example of the application of the method, consider $\mathrm{Tr}(\mathbf{T}/\lambda)^n$, the nth-order term in the summation in equation (11). This term is represented as the ring diagram displayed in figure 1. The large dot that separates the crosses representing the ηs at the two ends of the right-hand side of equation (13) is, like the other dots in the diagram, a representation of the component and labelled by i_k. The zeroth-order contribution to $\langle \mathrm{Tr}(\mathbf{T})/\lambda)^n \rangle$ is obtained by pairing off adjacent ηs only. The diagram representing this pairing is shown in figure 1(*b*). This diagram represents

$$\sum_{\substack{\alpha_1\beta_1 \\ \alpha_2\beta_2}} \frac{a_{\alpha_1\beta_1}}{\lambda} \delta_{\beta_1\alpha_2} \frac{a_{\alpha_2\beta_2}}{\lambda} \cdots \frac{a_{\alpha_n\beta_2}}{\lambda} \delta_{\beta_n\alpha_1} = \mathrm{Tr}\left(\frac{\mathbf{a}}{\lambda}\right)^n. \tag{16}$$

3. $\langle R(\lambda) \rangle$: $1/d^2$ contributions

In order to evaluate the $1/d^2$ correction to the resolvent, it proves convenient to separate the contribution into two classes, *irreducible* and *reducible* diagrams. Consider

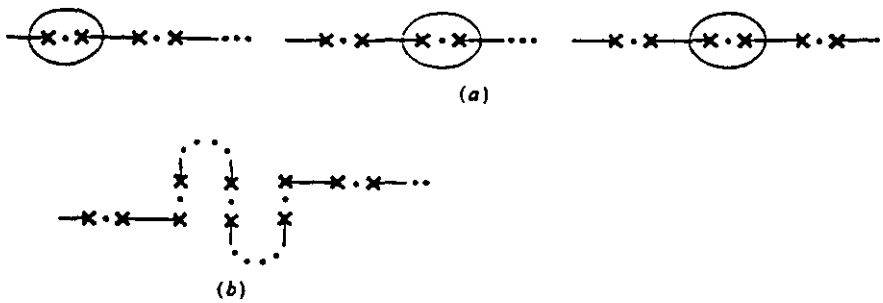

Figure 2. (*a*) Three sets of ηs in the diagrammatic representation of $(T/\lambda)^n$, shown encircled. (*b*) The three sets are pulled together as a preliminary step in the pairing of the ηs in the sets.

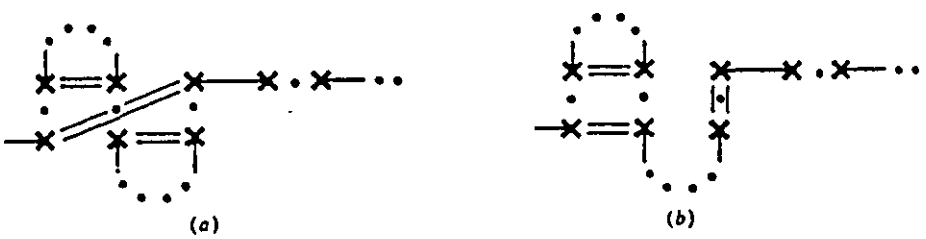

Figure 3. (*a*) The irreducible pairing of the ηs in the three sets brought together in figure 9(*b*). (*b*) A reducible pairing of the ηs in these sets.

for example the three sets of ηs in a chain, shown encircled in figure 2(*a*). The chain is 'bent' so that pairs are moved near to each other as in figure 2(*b*). Figure 3(*a*) displays an irreducible pairing of the six ηs in the three sets and figure 3(*b*) displays a reducible pairing of these six ηs. A diagram is irreducible when a pairing of the ηs in a group of n sets cannot be broken down into pairings between ηs in groups of n and $n-m$ sets where no pairings exist between an η in one group and an η in another.

3.1. Irreducible diagrams

Consider the kth, $(R+m)$th and $(k+m+r)$th pairs of figure 1, counting clockwise, and bring the 6ηs together as shown in figure 4.

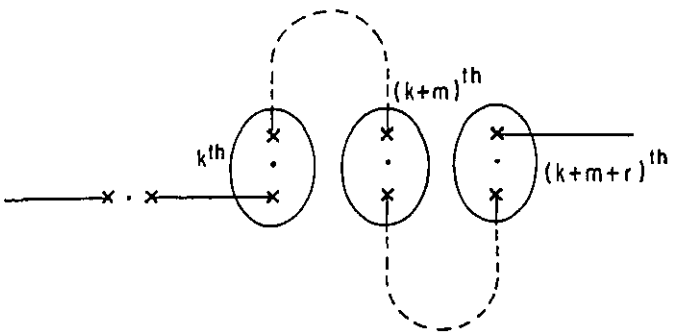

Figure 4. Three sets of ηs in the diagrammatic representation of $(T/\lambda)^n$ are shown encircled. The three sets are pulled together as a preliminary step in the pairing of non-adjacent ηs.

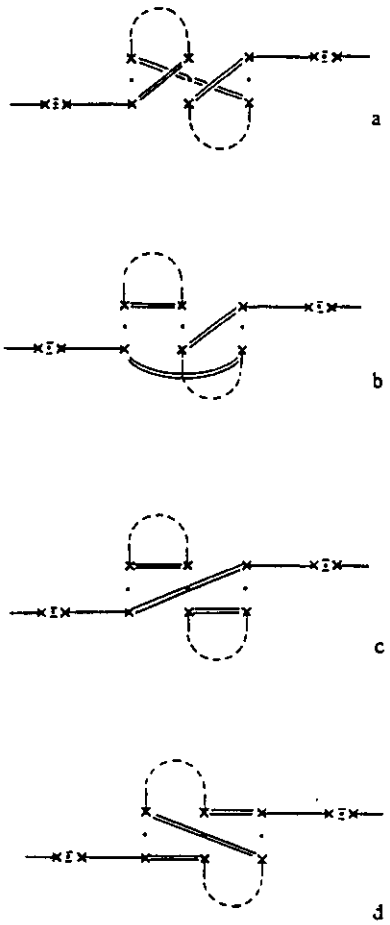

Figure 5. The four topologically distinct way of pairing the six ηs appearing in figure 4 are exhibited in (a)-(d).

The pairings of non-adjacent ηs occur between the kth, $(k+m)$th and $(k+m+r)$th pairs of the ηs pairs. The four ways of pairing them are displayed in figure 5$(a$-$d)$. If the remaining pairings are all of adjacent ηs, we obtain a contribution in $1/d^2$ to $1/\lambda\langle \mathrm{Tr}(\mathbf{T}/\lambda)^n\rangle$ from the irreducible pairings (see table 1). The reader is referred to the appendix for details of the calculation. Here we only give the final result. The total contribution from the irreducible diagrams to the resolvent function $\langle R(\lambda)\rangle$ is

$$\langle R(\lambda)\rangle_1 = \frac{1}{\lambda}\frac{1}{d^2}\sum_i 8\frac{\alpha_i^3}{(\lambda-\alpha_i)^4} + \frac{1}{\lambda}\frac{1}{d^2}\sum_{i\neq j\neq k}\frac{\alpha_i}{(\lambda-\alpha_i)^2}\frac{\alpha_j}{(\lambda-\alpha_j)}\frac{\alpha_k}{(\lambda-\alpha_k)}$$
$$+2\frac{1}{\lambda}\frac{1}{d^2}\left(\sum_{i\neq j}\frac{\alpha_i}{(\lambda-\alpha_i)^2}\frac{\alpha_j}{(\lambda-\alpha_j)^2}+\sum_{i\neq j}\frac{\alpha_i}{(\lambda-\alpha_i)}\frac{2\alpha_j^2}{(\lambda-\alpha_j)^3}\right). \tag{17}$$

3.2. Reducible diagrams

Similarly, we consider the kth, $(k+m)$th, $(k+m+n)$th and $(k+m+r+p)$th pairs of figure 4, counting clockwise. We bring the eight ηs together as shown in figure 6. The

Table 1. The contribution of the irreducible diagrams to $\mathrm{Tr}(T/\lambda)^n$.

Diagram		Contribution
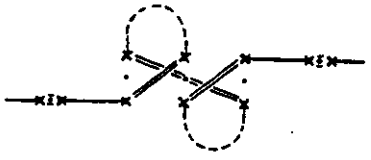	(a)	$\frac{1}{d^2}\frac{n(n-1)(n-2)}{2}\mathrm{Tr}\left(\frac{\mathbf{a}}{\lambda}\right)^n$
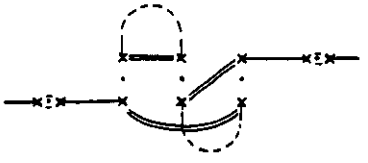	(b)	$\frac{1}{d^2}n(n-m-1)\,\mathrm{Tr}\left(\frac{\mathbf{a}}{\lambda}\right)^m \mathrm{Tr}\left(\frac{\mathbf{a}}{\lambda}\right)^{n-m}$
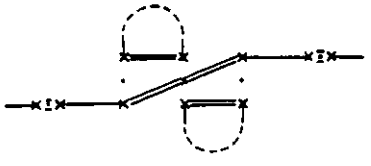	(c)	$\frac{1}{d^2}\frac{n}{3}\mathrm{Tr}\left(\frac{\mathbf{a}}{\lambda}\right)^m \mathrm{Tr}\left(\frac{\mathbf{a}}{\lambda}\right)^n \mathrm{Tr}\left(\frac{\mathbf{a}}{\lambda}\right)^{n-(m+r)}$
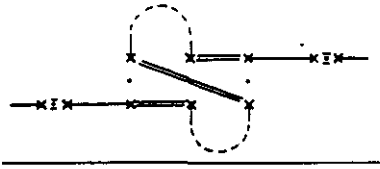	(d)	$\frac{1}{d^2}\frac{n(n-1)(n-2)}{6}\mathrm{Tr}\left(\frac{\mathbf{a}}{\lambda}\right)^n$

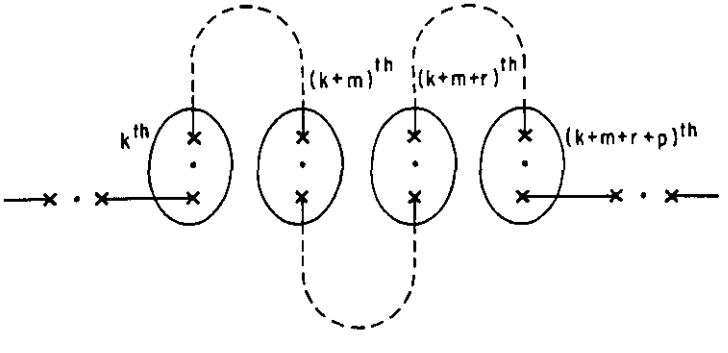

Figure 6. Four sets of ηs in the diagrammatic representation of $(\mathbf{T}/\lambda)^n$ are shown encircled. The four sets are pulled together as a preliminary step in the pairing of non-adjacent ηs.

$1/d^2$ correction term arises because of the pairings of non-adjacent ηs that occur between these pairs, and the six different ways of pairing them are displayed in figure $7(a\text{–}f)$. The remaining pairings are all of adjacent ηs. After summing all the contributions of the reducible diagrams to the resolvent function $\langle R(\lambda)\rangle$ (see table 2), we obtain

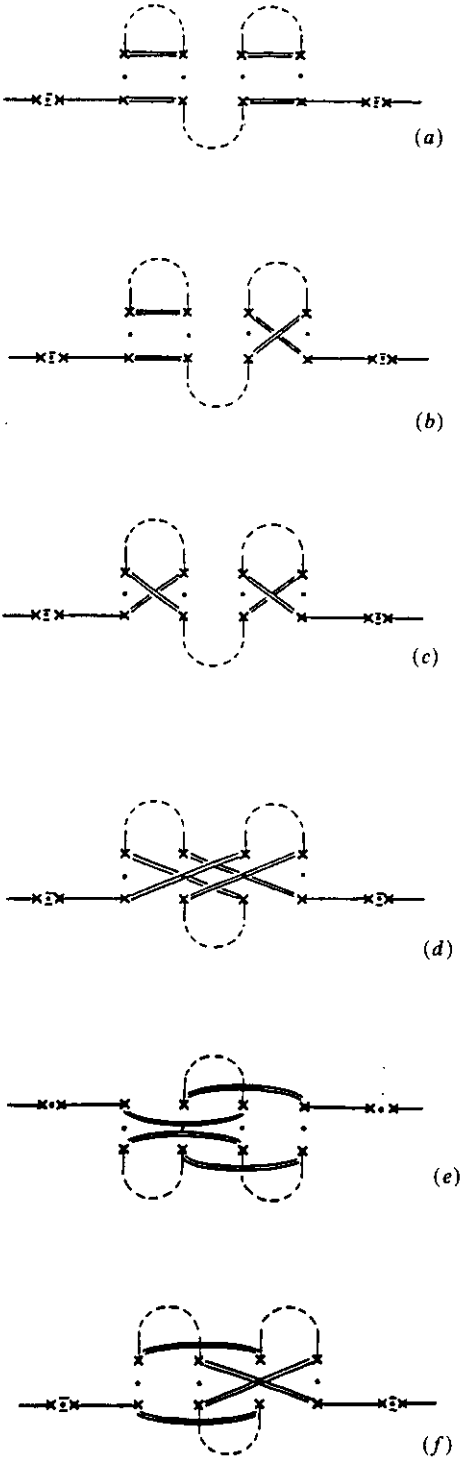

Figure 7. The six topologically distinct ways of pairing the light ηs appearing in figure 6 are exhibited in (a)-(f).

Table 2. The contribution of the reducible diagrams to $\mathrm{Tr}(\mathbf{T}/\lambda)^n$.

Diagram	Contribution
 (*a*)	$\frac{1}{d^2}\frac{n}{2}\mathrm{Tr}\left(\frac{\mathbf{a}}{\lambda}\right)^m \mathrm{Tr}\left(\frac{\mathbf{a}}{\lambda}\right)^p \mathrm{Tr}\left(\frac{\mathbf{a}}{\lambda}\right)^{n-(m+p)}$
 (*b*)	$\frac{1}{d^2} n \,\mathrm{Tr}\left(\frac{\mathbf{a}}{\lambda}\right)^m \mathrm{Tr}\left(\frac{\mathbf{a}}{\lambda}\right)^{n-m}$
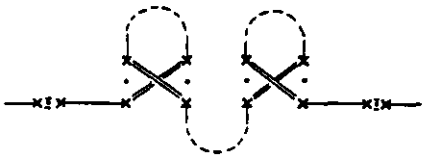 (*c*)	$\frac{1}{d^2}\frac{n}{2}\mathrm{Tr}\left(\frac{\mathbf{a}}{\lambda}\right)^n$
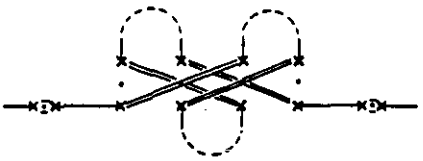 (*d*)	$\frac{1}{d^2}\frac{n}{4}\mathrm{Tr}\left(\frac{\mathbf{a}}{\lambda}\right)^n$
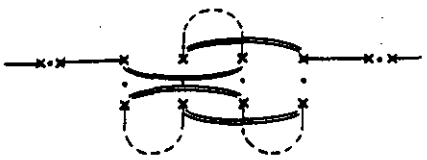 (*e*)	$\frac{1}{d^2}\frac{n}{2}\mathrm{Tr}\left(\frac{\mathbf{a}}{\lambda}\right)^n$
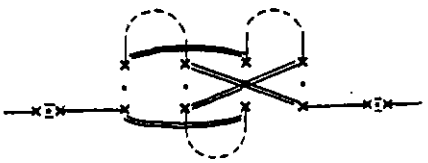 (*f*)	$\frac{1}{d^2}\frac{n}{4}\mathrm{Tr}\left(\frac{\mathbf{a}}{\lambda}\right)^{m+r} \mathrm{Tr}\left(\frac{\mathbf{a}}{\lambda}\right)^{n-(m+r)}$

the following result for the reducible contribution to the resolvent function:

$$\langle R(\lambda)\rangle_R = 12\frac{1}{\lambda}\frac{1}{d^2}\sum_i \frac{\alpha_i^4}{(\lambda-\alpha_i)^5} + 3\frac{1}{\lambda}\frac{1}{d^2}\sum_{i\neq j}\frac{\alpha_i^2}{(\lambda-\alpha_i)^3}\frac{\alpha_j^2}{(\lambda-\alpha_j)^2}$$
$$+2\frac{1}{\lambda}\frac{1}{d^2}\sum_{i\neq j}\frac{\alpha_i}{(\lambda-\alpha_i)^2}\frac{\alpha_j^3}{(\lambda-\alpha_j)^3} + 6\frac{1}{\lambda}\frac{1}{d^2}\sum_{i\neq j}\frac{\alpha_i}{(\lambda-\alpha_i)}\frac{\alpha_j^3}{(\lambda-\alpha_j)^4}$$
$$+\frac{1}{\lambda}\frac{1}{d^2}\sum_{i\neq j\neq k}\frac{\alpha_i}{(\lambda-\alpha_i)^2}\frac{\alpha_j}{(\lambda-\alpha_j)}\frac{\alpha_k^2}{(\lambda-\alpha_k)^2}$$
$$+\frac{1}{\lambda}\frac{1}{d^2}\sum_{i\neq j\neq k}\frac{\alpha_i}{(\lambda-\alpha_i)}\frac{\alpha_j}{(\lambda-d_j)}\frac{\alpha_k^2}{(\lambda-d_k)^3}. \tag{18}$$

Summing the irreducible and reducible contributions gives the total $1/d^2$ term in the expansion of the resolvent function, which, with the use of (9), yield the following result for the $1/d^2$ correction to the average principal radii of gyration:

$$\langle\Delta\lambda_i\rangle = \frac{1}{d^2}\sum_{j\neq i}\frac{\alpha_i^2\alpha_j^2}{(\alpha_i-\alpha_j)^3} = \frac{-\alpha_i i^4}{d^2}\sum_j \frac{j^2}{(i^2-j^2)^3}. \tag{19}$$

The sum on the left-hand side of this equation can be carried out exactly using contour integration methods. We find

$$\sum_{j(j\neq i)}^{\infty}{}' \frac{j^2}{(i^2-j^2)^3} = \frac{1}{32i^4} - \frac{\pi^2}{48i^2}. \tag{20}$$

Thus, our final result for $\langle\lambda_i\rangle$ to order $1/d^2$ is

$$\langle\lambda_i\rangle = \alpha_i\left[1+\frac{3}{4d}+\frac{1}{d^2}\left(\frac{\pi^2 i^2}{48}-\frac{1}{32}\right)\right]+O\left(\frac{1}{d^3}\right) \tag{21}$$

where the zeroth-order term

$$\alpha_i = \frac{(N+1)}{\pi^2 i^2} \qquad 1\leq i\leq d. \tag{22}$$

The $O(1/d)$ contribution to equation (21) was previously derived (Rudnick *et al* 1987, Gaspari *et al* 1987).

Following the procedures outlined above, we find that the $1/d^2$ contribution term to the average of the square of the eigenvalue, $\langle\lambda_i^2\rangle$, is given by

$$\langle\Delta\lambda_i^2\rangle = -4\frac{1}{d^2}\sum_{\substack{j\\(j\neq i)}}\frac{\alpha_i^3\alpha_j}{(\alpha_i-\alpha_j)} + 2\frac{1}{d^2}\sum_{\substack{j\\(j\neq i)}}\frac{\alpha_i^2\alpha_j}{(\alpha_i-\alpha_j)}$$
$$+2\frac{1}{d^2}\left(\sum_{\substack{j\\(j\neq i)}}\frac{\alpha_i^4\alpha_j}{(\alpha_i-\alpha_j)^3}+\frac{1}{d^2}\alpha_i^2\sum_{\substack{j\\(j\neq i)}}\frac{\alpha_j}{(\alpha_i-\alpha_j)}\right)^2. \tag{23}$$

We make use of the following results:

$$\sum_{\substack{j\\(j\neq i)}}\frac{1}{(j^2-i^2)} = -\frac{3}{4}\frac{1}{i^2}$$
$$\sum_{\substack{j\\(j\neq i)}}\frac{1}{(j^2-i^2)^2} = \frac{\pi^2}{12i^2}-\frac{11}{16}\frac{1}{i^4} \tag{24}$$
$$\sum_{\substack{j\\(j\neq i)}}\frac{j^2}{(j^2-i^2)^3} = \frac{\pi^2}{48}\frac{1}{i^2}-\frac{1}{32}\frac{1}{i^4}.$$

The $1/d^2$ correction term becomes

$$\langle \Delta\lambda_i^2 \rangle_{1/d^2} = \frac{1}{d^2}\alpha_i^2\left(\frac{\pi^2 i^2}{8}+\frac{7}{4}\right). \tag{25}$$

Finally, we obtain to order $1/d^2$:

$$\langle \lambda_i^2 \rangle = \left(\frac{(N+1)}{\pi^2 i^2}\right)^2\left[1+\frac{7}{2}\frac{1}{d}+\frac{1}{d^2}\left(\frac{\pi^2}{8}i^2+\frac{7}{4}\right)\right]+\mathrm{O}\left(\frac{1}{d^3}\right). \tag{26}$$

The variance of the distribution is given by

$$\langle (\lambda_i - \langle \lambda_i \rangle)^2 \rangle = \left(\frac{(N+1)}{\pi^2 i^2}\right)^2\left[\frac{2}{d}+\frac{1}{d^2}\left(\frac{\pi^2}{12}i^2+\frac{9}{4}\right)\right]+\mathrm{O}\left(\frac{1}{d^3}\right) \tag{27}$$

and the ratios of the eigenvalues are

$$\frac{\langle \lambda_i \rangle}{\langle \lambda_j \rangle} = \frac{j^2}{i^2}\left(1+\frac{1}{d^2}\frac{\pi^2}{48}(i^2-j^2)\right). \tag{28}$$

From equation (28) we note that the ratios of the eigenvalues for linear chains depend on the spatial dimensions at order $1/d^2$.

4. Comparison with numerical simulations

There is no experimental data to compare with our $1/d$ expansion-predicted results; however, there exist numerical simulations. Here, we consider two sets of data. The first consists of data obtained by Bishop and Saltiel (1986), and Bishop and Michel (1986), where the shapes of linear and ring polymers, with and without excluded volume, were investigated numerically via Brownian dynamics in a variety of spatial dimensions. In their polymer model, N beads are joined together by nearest-neighbour harmonic spring forces, and each bead is subject to a random force and a frictional force proportional to the velocity. The other set consists of data we have generated for open walks. The two sources of data utilize different ways of exploring random walk configurations. In our theoretical study of shapes of random walks, there was no interaction between bonds nor were any other forces taken in consideration. The advantage of using our method of generating random walk configurations is its direct relation to the real random walk process, and the fact that it is an efficient algorithm to generate walks of very large number of steps. The advantage of using the data obtained by Bishop and co-workers is that their model is closer to the nature of real polymers. In addition, they were able to study ring polymers as well.

Before proceeding with the comparison between our $1/d$ expansion-predicted results and the numerical calculations, we test both sources of data using exact analytical results for the square of the radius of gyration open walks.

4.1. Average radius of gyration $\langle R^2 \rangle$

Recall that the analytical formula for the square of the radius of gyration $\langle R^2 \rangle = \sum_{i=1}^{d} \langle \lambda_i \rangle$ is an exact result and is given by $\langle R^2 \rangle = (N+1)/6$ for an N-step open walk or linear chain and by $\langle R^2 \rangle = (N+1)/12$ for an N-step closed walk or polymer ring (Kramers 1946, Zimm and Stockmeyer 1949).

Table 3. Eigenvalues $\langle\lambda_i\rangle$ and their ratios for linear chains. Comparison between $1/d$ expansion and exact results and numerical calculations for an $N = 100$-step walk.

Dimension (d)	Eigenvalue	$1/d$ expansion theoretical results ($N = 100$)			Numerical results
		0th order	1st order	2nd order	
2	$\langle\lambda_1\rangle$	10.233	14.071	14.517	14.269
	$\langle\lambda_2\rangle$	2.558	3.518	4.023	2.779
	$\langle\lambda_1\rangle/\langle\lambda_2\rangle$	4.00	4.00	3.383	5.134
	$\langle R^2\rangle$	101/6 = 16.83	101/6 = 16.83	101/6 = 16.83	17.048
3	$\langle\lambda_1\rangle$	10.233	12.792	12.990	12.925
	$\langle\lambda_2\rangle$	2.558	3.198	3.423	2.873
	$\langle\lambda_3\rangle$	1.137	1.421	1.651	1.042
	$\langle\lambda_1\rangle:\langle\lambda_2\rangle:\langle\lambda_3\rangle$	9:2.25:1	9:2.25:1	7.35:1.99:1	12.404:2.757:1
	$\langle\lambda_1\rangle/\langle\lambda_2\rangle$	4.00	4.00	3.726	4.498
	$\langle R^2\rangle$	101/6 = 16.83	101/6 = 16.83	101/6 = 16.83	16.84

We have tested our numerical simulations for the open walk against these exact results. For an $N = 100$-step walk, the difference between our data and the exact results is about 1.26% in two dimensions and 0.04% in three dimensions. The agreement is very good. We are thus encouraged to compare the $1/d$ expansion-predicted results with our numerical calculations. This comparison is displayed in table 3.

The data obtained by Bishop and Saltiel (1986) for the eigenvalues of the radius of gyration tensor were also tested by comparing their numerical result for the average

Table 4. Eigenvalues $\langle\lambda_i\rangle$ and their ratios for linear chains. Comparison between $1/d$ expansion and exact results and numerical calculations of Bishop and Saltiel for an $N = 32$-step walk.

Dimension (d)	Eigenvalue	$1/d$ expansion theoretical results ($N = 32$)			Numerical results
		0th order	1st order	2nd order	
2	$\langle\lambda_1\rangle$	3.343	4.597	4.743	4.81 ± 0.28
	$\langle\lambda_2\rangle$	0.835	1.149	1.314	0.92 ± 0.53
	$\langle\lambda_1\rangle/\langle\lambda_2\rangle$	4.00	4.00	3.383	5.22
	$\langle R^2\rangle$	33/6 = 5.5	33/6 = 5.5	33/6 = 5.5	5.73
4	$\langle\lambda_1\rangle$	3.343	3.970	4.007	4.04 ± 0.28
	$\langle\lambda_2\rangle$	0.835	0.992	1.033	0.96 ± 0.03
	$\langle\lambda_3\rangle$	0.371	0.441	0.483	0.38 ± 0.01
	$\langle\lambda_4\rangle$	0.203	0.248	0.290	0.18 ± 0.01
	$\langle\lambda_1\rangle/\langle\lambda_2\rangle$	4.00	4.00	3.845	4.20
	$\langle R^2\rangle$	33/6 = 5.5	33/6 = 5.5	33/6 = 5.5	5.56
5	$\langle\lambda_1\rangle$	3.343	3.845	3.868	3.95 ± 0.17
	$\langle\lambda_2\rangle$	0.835	0.961	0.987	0.99 ± 0.05
	$\langle\lambda_3\rangle$	0.371	0.427	0.454	0.37 ± 0.02
	$\langle\lambda_4\rangle$	0.209	0.240	0.267	0.19 ± 0.04
	$\langle\lambda_5\rangle$	0.133	0.153	0.181	0.11 ± 0.001
	$\langle\lambda_1\rangle/\langle\lambda_2\rangle$	4.00	4.00	3.901	3.99
	$\langle R^2\rangle$	33/6 = 5.5	33/6 = 5.5	33/6 = 5.5	5.61

radius of gyration with the exact result. For an $N = 32$-step walk, using their numerical results as displayed in table 4, one finds a discrepancy between their numbers and the exact result for the average radius of gyration of about 4% in two dimensions, 1% in four dimensions and 2% in five dimensions. Again, there is good agreement between their data and the exact result.

4.2. *Eigenvalues $\langle\lambda_i\rangle$ and their ratios: comparison of $1/d^2$ expansion with numerical results*

In the previous sections, we were able to obtain the analytical expression for the average principal radii of gyration of an open walk embedded in d-spatial dimensions. We found that, to second order in $1/d$, the ith eigenvalue is given by

$$\langle\lambda_i\rangle = \frac{(N+1)}{\pi^2 i^2}\left[1+\frac{3}{4d}+\frac{1}{d^2}\left(\frac{\pi^2 i^2}{48}-\frac{1}{32}\right)\right]+O\left(\frac{1}{d^3}\right) \tag{29}$$

and that the ratio of the eigenvalues is

$$\frac{\langle\lambda_i\rangle}{\langle\lambda_j\rangle} = \frac{j^2}{i^2}\left(1+\frac{1}{d^2}\frac{\pi^2}{48}(i^2-j^2)\right). \tag{30}$$

Table 3 contains a comparison between predictions based on equations (29) and (30) and our numerical data. Table 4 displays another comparison between the theoretical predictions with the numerical calculations of Bishop and Saltiel (1986).

First reconsider the eigenvalues of the radius of gyration tensor themselves. Considering the largest eigenvalues only, in comparing our simulations, the error difference between the two findings in $d = 3$ is about 20% at zeroth order in $1/d$ and decreases to 0.5% when one includes the second-order term of the $1/d$ expansion. The agreement is excellent even for a small number of steps and at relatively low spatial dimensionality. In two dimensions, the error difference for the largest eigenvalue decreases from 28% at zeroth order to slightly less than 2% when one includes the next higher-order terms.

By contrast, considering the lowest eigenvalues, agreement between our predictions and the numerical results becomes worse as one includes higher-order terms of the $1/d$ expansion. In three dimensions, from the comparison in table 3, the error difference between the two results increases from 8.3% at zeroth order of the expansion to 36% when one includes the second-order term in $1/d$. A possible explanation is as follows. Our eigenvalues will generally have overlapping distributions, as displayed in figure 8. Suppose one of the eigenvalues, α_1, has a larger average than α_2, i.e. $\langle\alpha_1\rangle > \langle\alpha_2\rangle$. The eigenvalue associated with the distribution closer to the origin can be larger than the eigenvalue associated with the distribution further out, especially in the overlap region indicated in figure 8. However, our method will always identify the second eigenvalue above as the larger one because our analysis is based on an expansion about $d = \infty$ delta function distributions. It is clear that the overlap region covers most of the entire portion of the curve of the 'smaller' eigenvalue, but it only covers a small portion of the curve of the 'larger' eigenvalue. Therefore, the overlap will have a stronger effect on the smaller eigenvalue. The extent to which these peaks overlap will be discussed later.

A similar comparison of the eigenvalues of the radii of gyration tensor for linear chains can be made using the data obtained by Bishop and Saltiel and is displayed in table 4. The trends are found to be similar. In two dimensions, the agreement, in the case of λ_1, is improved as the highest-order terms of the $1/d$ expansion are included. There is a systematic improvement for the largest eigenvalue in every dimension.

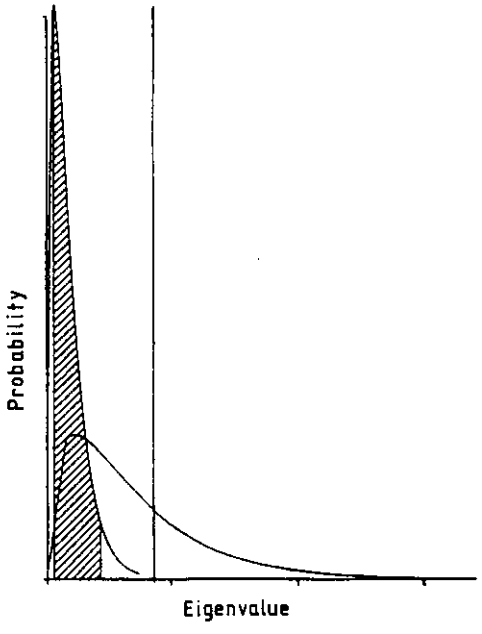

Figure 8. Probability distributions for the largest eigenvalue ($P_1(\alpha_1)$) and for the smallest eigenvalue ($P_2(\alpha_2)$) as given by equation (31) for 100-step walks in three dimensions.

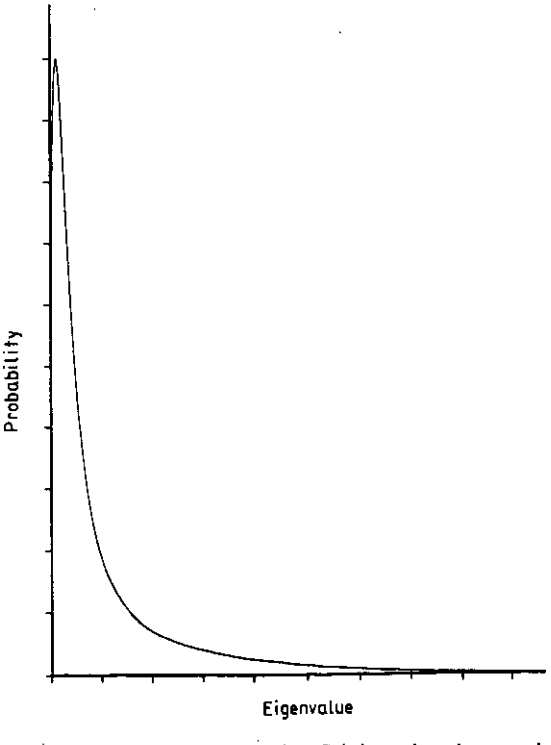

Figure 9. Probability distribution $P_i(\lambda)$ as given by equation (31) in three dimensions for 100-step walks.

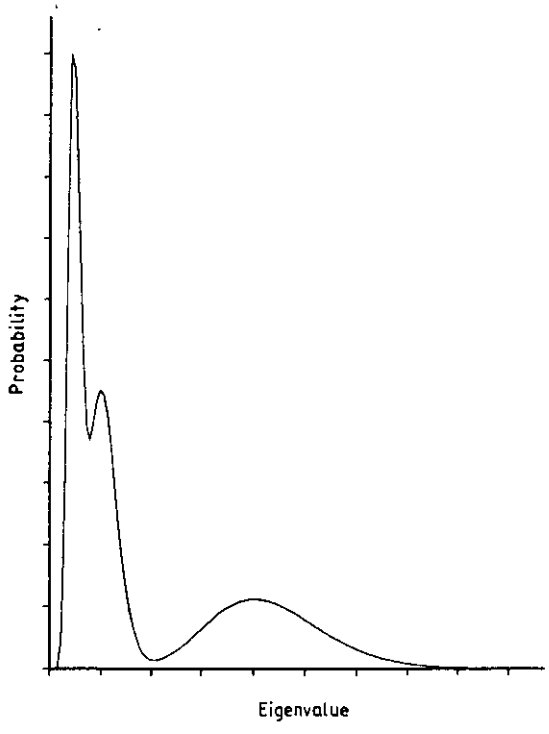

Figure 10. Probability distribution $P_i(\lambda)$ as given by equation (31) in 30 dimensions for 100-step walks.

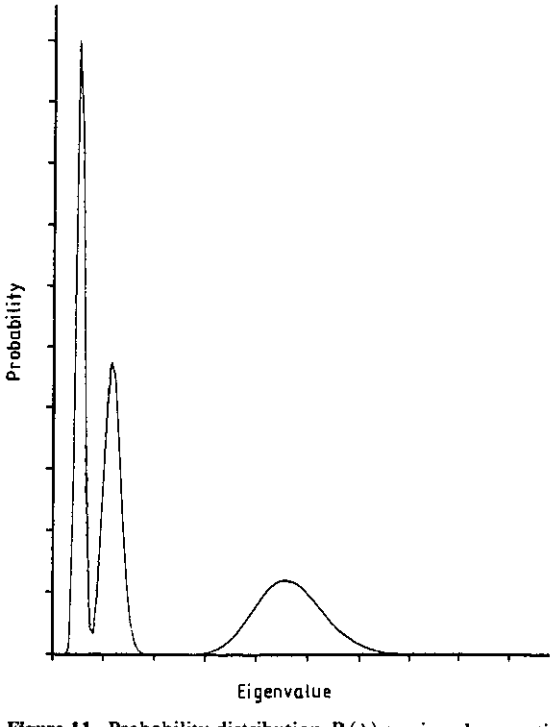

Figure 11. Probability distribution $P_i(\lambda)$ as given by eqaution (31) in $d = 100$ for 100-step walks.

When comparing the *ratios* of the eigenvalues, the predictions are worse in two dimensions as expected. Higher-order corrections lead to the poorer agreement and this is probably due to the previously discussed overlap of the distribution that is not taken into account in this expansion. The agreement gets better as the dimension increases. In five dimensions, the difference between the data and the predictions of the $1/d$ expansion is about 2.2% and the result is well within the error bar.

4.3. Probability distribution of the principal radii of gyration in various spatial dimensions

In this section, we investigate the behaviour of the distribution function for the individual principal components of the radius of gyration in various spatial dimensions. This will provide information about the behaviour of the resolvent $\langle R(\lambda)\rangle$ between consecutive eigenvalues and its peaks in these intervals. The analysis is carried out numerically. The results indeed show that there is only a single peak at low dimensions. Figure 9 displays the curve of the probability distribution $P(\lambda)$ against the eigenvalue λ in three dimensions where $P(\lambda)=P_1(\lambda)+P_2(\lambda)+P_3(\lambda)$ with $P_i(\lambda)$ are defined as obtained before in our previous paper (Gaspari *et al* 1986). They satisfy

$$P_i(\lambda)=C_i\left(\frac{\lambda}{\alpha_i}\right)^{(d/2)-1}\exp\left(-\frac{d}{2}\frac{\lambda}{\alpha_i}\right) \tag{31}$$

where the quantity C_i is adjusted to normalize the probability distribution $P_i(\lambda)$ to 1.

It is clear that there exists only one peak in three dimensions. In other words the peaks that correspond to the total distribution overlap at lower dimensionality. These peaks start to be well separated only in relatively high spatial dimensions. For instance, figure 10 shows the separation of the peaks for the largest and next-largest eigenvalues in 30 dimensions. The existence of the three well separated peaks, as shown in figure 11, occurs at very high dimensions ($d=100$).

Our method of extracting the eigenvalues up to any higher order in $1/d$ assumes that the imaginary part of the averaged resolvent $\langle R(\lambda)\rangle$, is very small in some interval between consecutive eigenvalues and therefore this quantity has very well-separated peaks. However, as we have seen, this condition is satisfied only at high dimensions. In lower dimensionality, the existence of only one peak represents a limitation on the accuracy of the $1/d$ expansion for any but the largest eigenvalue; this is indeed verified when comparing the predictions of the $1/d$ expansion to second order in $1/d$ for the smaller eigenvalues with the numerical results.

Appendix

In this appendix we illustrate how the resolvent function $\langle R(\lambda)\rangle$ is obtained to order $1/d^2$ using the diagrammatical method. We consider here only one diagram (figure 5(b)). The same analysis is used for the others.

The double lines represent pair averages. For instance, the irreducible pairings of the ηs in the three sets yield

$$\langle \eta_{\beta_{k-1}i_k}\eta_{\beta_{k+m-1}i_{k+m}}\rangle=\frac{1}{d}\,\delta_{\alpha_k\beta_{k+m-1}}\delta_{i_ki_{k+m}}. \tag{A1}$$

The remaining pairings are all of adjacent ηs. By careful consideration of the effects of the delta functions generated by these pairings, we arrive at the following result for the contribution of this diagram to $\langle \mathrm{Tr}(\mathbf{T}/\lambda)^n \rangle$:

$$Tr\left(\frac{\mathbf{a}}{\lambda}\right)^m \mathrm{Tr}\left(\frac{\mathbf{a}}{\lambda}\right)^{n-m} \sum_{\substack{i_k=1 \\ i_{k+m}=1 \\ i_{k+m+r}=1}} \frac{1}{d^3} \delta_{i_k i_{k+m}} \delta_{i_k i_{k+m+r}} \delta_{i_{k+m} i_{k+m+r}} \tag{A2}$$

which is just

$$\frac{1}{d^2} \mathrm{Tr}\left(\frac{\mathbf{a}}{\lambda}\right)^m \mathrm{Tr}\left(\frac{\mathbf{a}}{\lambda}\right)^{n-m}.$$

As can be established by inspection, the number of different ways of forming this diagram is $n(n-m-1)$. Therefore its total contribution to $\langle \mathrm{Tr}(\mathbf{T}/\lambda)^n \rangle$ is

$$\begin{aligned} & n(n-m-1) \frac{1}{d^2} \mathrm{Tr}\left(\frac{\mathbf{a}}{\lambda}\right)^m \mathrm{Tr}\left(\frac{\mathbf{a}}{\lambda}\right)^{n-m} \\ & \quad = \frac{1}{d^2} n(n-m-1) \sum_{i,j} \left(\frac{\alpha_i}{\lambda}\right)^m \left(\frac{\alpha_j}{\lambda}\right)^{n-m} \\ & \quad = \frac{1}{d^2} n(n-m-1) \sum_{\substack{i,j \\ i \neq j}} \left(\frac{\alpha_i}{\lambda}\right)^m \left(\frac{\alpha_j}{\lambda}\right)^{n-m} + \frac{1}{d^2} n(n-m-1) \sum_i \left(\frac{\alpha_i}{\lambda}\right)^n. \end{aligned} \tag{A3}$$

Now we sum over all 'locations' of the non-adjacent pairings and obtain

$$\frac{1}{d^2} \sum_{i \neq j} \sum_{n=1}^{\infty} \sum_{m=1}^{n-1} n(n-m-1) \left(\frac{\alpha_i}{\lambda}\right)^m \left(\frac{\alpha_j}{\lambda}\right)^{n-m} + \frac{1}{d^2} \sum_i \sum_{n=1}^{\infty} \sum_{m=1}^{n-1} n(n-m-1) \left(\frac{\alpha_i}{\lambda}\right)^m \left(\frac{\alpha_i}{\lambda}\right)^{n-m}.$$

Using standard results for geometrical series, we find that the final contribution to $\langle \mathrm{Tr}(\mathbf{T}/\lambda)^n \rangle$ of the diagram becomes

$$\begin{aligned} & \frac{1}{d^2} \sum_i 3 \frac{(\alpha_i/\lambda)^3}{[1-(\alpha_i/\lambda)]^4} + \frac{1}{d^2} \sum_{i \neq j} \frac{(\alpha_i/\lambda)}{[1-(\alpha_i/\lambda)]^2} \frac{(\alpha_j/\lambda)^2}{[1-(\alpha_j/\lambda)]^2} \\ & \qquad + \frac{1}{d^2} \sum_{i \neq j} \frac{(\alpha_i/\lambda)}{[1-(\alpha_i/\lambda)]} \frac{2(\alpha_j/\lambda)^2}{[1-(\alpha_j/\lambda)]^3}. \end{aligned} \tag{A4}$$

A similar analysis can be carried for all diagrams contributing to $\langle \mathrm{Tr}(\mathbf{T}/\lambda)^n \rangle$. Here we consider only the ones contributing to $1/d^2$ corrections. The expressions assigned to each diagram are listed below.

Contribution from figure 5(a):

$$\frac{1}{d^2} \sum_i 3 \frac{(\alpha_i/\lambda)^3}{[1-(\alpha_i/\lambda)]^4}. \tag{A5}$$

Contribution from figure 5(c):

$$\begin{aligned} & \frac{1}{d^2} \sum_i \frac{(\alpha_i/\lambda)^3}{[1-(\alpha_i/\lambda)]^4} + \frac{1}{d^2} \sum_{i \neq j \neq k} \frac{(\alpha_i/\lambda)}{[1-(\alpha_i/\lambda)]^2} \frac{(\alpha_j/\lambda)}{[1-(\alpha_j/\lambda)]} \frac{(\alpha_k/\lambda)}{[1-(\alpha_k/\lambda)]} \\ & \qquad + \frac{1}{d^2} \sum_{i \neq j} \left(2 \frac{(\alpha_i/\lambda)^2 (\alpha_j/\lambda)}{[1-(\alpha_i/\lambda)]^3 [1-(\alpha_j/\lambda)]} + \frac{(\alpha_i/\lambda)^2 (\alpha_j/\lambda)}{[1-(\alpha_i/\lambda)]^2 [1-(\alpha_j/\lambda)]^2} \right). \end{aligned} \tag{A6}$$

Contribution from figure 5(d):

$$\frac{1}{d^2}\sum_i \frac{(\alpha_i/\lambda)^3}{[1-(\alpha_i/\lambda)]^4}. \tag{A7}$$

Similarly we obtain the following results from the reducible diagrams.
Contribution from (a) in table 2:

$$\frac{1}{d^2}\sum_i 2\frac{(\alpha_i/\lambda)^4}{[1-(\alpha_i/\lambda)]^5}+\frac{1}{d^2}\sum_{i\neq j} 2\frac{(\alpha_i/\lambda)^2}{[1-(\alpha_i/\lambda)]^3}\frac{(\alpha_j/\lambda)^2}{[1-(\alpha_j/\lambda)]^2}$$
$$+\frac{1}{d^2}\left(\sum_{i\neq j}\frac{(\alpha_i/\lambda)}{[1-(\alpha_i/\lambda)]^2}\frac{(\alpha_j/\lambda)}{[1-(\alpha_j/\lambda)]^3}+\sum_{i\neq j} 3\frac{(\alpha_i/\lambda)}{[1-(\alpha_i/\lambda)]}\frac{(\alpha_j/\lambda)^3}{[1-(\alpha_j/\lambda)]^4}\right)$$
$$+\frac{1}{d^2}\sum_{i\neq j\neq k}\frac{(\alpha_i/\lambda)(\alpha_j/\lambda)(\alpha_k/\lambda)^2}{[1-(\alpha_i/\lambda)][1-(\alpha_j/\lambda)][1-(\alpha_k/\lambda)]^3}. \tag{A8}$$

Contribution from (b):

$$\frac{1}{d^2}\sum_i 4\frac{(\alpha_i/\lambda)^4}{[1-(\alpha_i/\lambda)]^5}+\frac{1}{d^2}\sum_{i\neq j}\frac{(\alpha_i/\lambda)}{[1-(\alpha_i/\lambda)]^2}\frac{(\alpha_j/\lambda)^3}{[1-(\alpha_j/\lambda)]^3}$$
$$+\frac{1}{d^2}\sum_{i\neq j} 3\frac{(\alpha_i/\lambda)(\alpha_j/\lambda)^3}{[1-(\alpha_i/\lambda)][1-(\alpha_i/\lambda)]^4}. \tag{A9}$$

Contribution from (c):

$$\frac{1}{d^2}\sum_i 2\frac{(\alpha_i/\lambda)^4}{[1-(\alpha_i/\lambda)]^5}. \tag{A10}$$

Contribution from (d):

$$\frac{1}{d^2}\sum_i \frac{(\alpha_i/\lambda)^4}{[1-(\alpha_i/\lambda)]^5}. \tag{A11}$$

Contribution from (e):

$$\frac{1}{d^2}\sum_i 2\frac{(\alpha_i/\lambda)^4}{[1-(\alpha_i/\lambda)]^5}. \tag{A12}$$

Contribution from (f):

$$\frac{1}{d^2}\sum_i \frac{(\alpha_i/\lambda)^4}{[1-(\alpha_i/\lambda)]^5}+\frac{1}{d^2}\sum_{i\neq j}\frac{(\alpha_i/\lambda)^2}{[1-(\alpha_i/\lambda)]^3}\frac{(\alpha_j/\lambda)^2}{[1-(\alpha_j/\lambda)]^2}. \tag{A13}$$

References

Beldjenna A 1990 PhD Thesis, University of California, Los Angeles
Bishop M and Michel J P J 1985 *J. Chem. Phys.* **82** 1059
—— 1986 *J. Chem. Phys.* **85** 1074
Bishop M and Saltiel C 1986 *J. Chem. Phys.* **85** 6728 and references therein
Eichinger B E 1985 *Macromolecules* **18** 211
Fixman M 1962 *J. Chem. Phys.* **36** 306
Flory P J 1969 *Statistics of Chain Molecules* (New York: Interscience)
—— 1971 *Principles of Polymer Physics* (Ithaca, NY: Cornell University Press)
Forsman W and Hughes R 1963 *J. Chem. Phys.* **38** 2118

Gaspari G, Rudnick J and Beldjenna A 1987 *J. Phys. A: Math. Gen.* **20** 3393
Kramers H A 1946 *J. Chem. Phys.* **14** 415
Kuhn W 1936 *Kolloid Z.* **76** 258
—— 1939 *Kolloid Z.* **81** 3
Rudnick J and Gaspari G 1986 *J. Phys. A: Math. Gen.* **19** L191
Rudnick J, Beldjenna A and Gaspari G 1987 *J. Phys. A: Math. Gen.* **20** 971
Shy L Y and Eichinger E B 1989 *J. Chem. Phys.* **90** 5179
Solc K 1971 *J. Chem. Phys.* **55** 335
Zimm B H and Stockmeyer W 1949 *J. Chem. Phys.* **17** 1301